

Experimental evidence by neutron scattering of a crossover from Gaussian to non-Gaussian behavior in the α relaxation of polyisoprene

A. Arbe, J. Colmenero,* and F. Alvarez[†]*Unidad Física de Materiales (CSIC-UPV/EHU), Apartado 1072, 20080 San Sebastián, Spain*

M. Monkenbusch and D. Richter

Institut für Festkörperforschung, Forschungszentrum Jülich GmbH, D-52425 Jülich, Germany

B. Farago and B. Frick

Institut Laue-Langevin, Boîte Postale 156, 38042 Grenoble Cedex 9, France

(Received 19 December 2002; published 9 May 2003)

We report incoherent quasielastic neutron scattering experiments exploring the α -relaxation range in polyisoprene over an unprecedented range in momentum transfer Q . The data corroborate and validate earlier molecular dynamics simulations and reveal the existence of a crossover from Gaussian to non-Gaussian character of the main chain protons self-correlation function in the α -relaxation regime. The real challenge of the experiment was to push the neutron techniques to cover a Q range as wide as possible. By combining two neutron spin echo spectrometers and a backscattering instrument, we have been able to study the dynamics in a Q range of $0.1 \leq Q \leq 4.7 \text{ \AA}^{-1}$. In the low- Q regime the shape of the relaxation function was found to be related to the dispersion of the relaxation times as predicted by the Gaussian assumption. At short distances or large Q , this relationship is strongly violated indicating a non-Gaussian regime. We have performed a detailed comparison between the experiments and simulations at different temperatures and found, apart from a temperature shift, complete agreement. Combining experiments and simulations led to a consistent interpretation in terms of a distribution of jumps underlying the diffusive motion of protons in the α process. This model leads to a time-dependent non-Gaussianity parameter that agrees nearly quantitatively with the simulations and exhibits all features resolved so far from various simulations.

DOI: 10.1103/PhysRevE.67.051802

PACS number(s): 61.41.+e, 61.12.Ex, 64.70.Pf

I. INTRODUCTION

The exploration of the molecular processes underlying the glass transition is still a topic of great theoretical and experimental efforts. Atomistic information on the dynamics taking place in the supercooled liquid state—the α relaxation—can be obtained by quasielastic neutron scattering. In particular, the direct microscopic observation of the structural relaxation in glass-forming systems is realized by studying the behavior of the dynamic structure factor at its first maximum, which is due to the correlations between the structural units. In the case of polymer systems, such experiments are carried out with neutron spin echo (NSE) spectroscopy on fully deuterated samples. Further insight is obtained by incoherent scattering at protonated materials. The incoherent intensity relates to the self-part of the van Hove correlation function $G_s(\vec{r}, t)$ of the hydrogens in the system. $G_s(\vec{r}, t)$ is the probability to find an atom at time t at a position \vec{r} if it was at $\vec{r}=\vec{0}$ for $t=0$. Its Fourier transform in the space domain, the intermediate scattering function $S_{self}(Q, t)$, can

be accessed by NSE techniques; finally, the counterpart in the frequency domain, the incoherent scattering function $S_{self}(Q, \omega)$ is accessible by, e.g., time of flight (TOF) or backscattering (BS) techniques [1]. Here, $\hbar Q$ and $\hbar \omega$ are the momentum and energy transfer in the scattering experiment, respectively.

The development of computer simulation techniques has facilitated additional insight into this problem, since the trajectories of the moving entities in the supercooled liquid regime can be followed directly in real space. Calculations of observables e.g., mean squared displacements or non-Gaussian parameters have become possible. In a recent work [2], some of us have carried out fully atomistic molecular dynamics (MD) simulations on a polyisoprene (PI) model at 363 K, i.e., at about 150 K above the experimental glass transition temperature of this polymer ($T_g = 210$ K). Among other correlation functions, the intermediate self-correlation function $S_{self}(Q, t)$ for the main chain protons was calculated. $S_{self}(Q, t)$ displays a two-step decay, the slower of which is associated with the α relaxation. Following the commonly used experimental evaluation procedure, the slow relaxation step of $S_{self}(Q, t)$ was described in terms of a Kohlrausch-Williams-Watts (KWW) function:

$$S_{self}(Q, t) = A(Q) \exp \left[- \left(\frac{t}{\tau_w} \right)^\beta \right]. \quad (1)$$

Here, β is the stretching parameter describing the shape of the relaxation function ($0 < \beta \leq 1$) and τ_w the relaxation

*Also at Departamento de Física de Materiales, Universidad del País Vasco and Donostia International Physics Center, Apartado 1072, 20080 San Sebastián, Spain. Electronic address: wapcolej@sc.ehu.es

[†]Also at Departamento de Física de Materiales, Universidad del País Vasco, Apartado 1072, 20080 San Sebastián, Spain.

time which may depend on Q . $A(Q)$ is a generalized Lamb-Mössbauer-factor (LMF) accounting for the first fast decay of $S_{self}(Q,t)$,

$$A(Q) = \exp\left(-\frac{\langle u^2 \rangle}{3} Q^2\right), \quad (2)$$

where $\langle u^2 \rangle$ is the mean squared displacement associated to the fast decay step. In the Q range below Q_{max} (the Q value where the static structure factor shows its first maximum) the KWW relaxation time τ_w was found to follow a power law in Q

$$\tau_w \propto Q^{-2/\beta}. \quad (3)$$

This power law results from a Gaussian form of both, the self-part of the van Hove correlation function $G_s(r,t)$ and its Fourier transform $S_{self}(Q,t)$ [3]. For $Q < Q_{max}$, such a power law relationship has been found experimentally for different polymers (see, e.g., [3–5]). For $Q > Q_{max}$, strong deviations from this Gaussian behavior manifest in the simulations (see also Ref. [6]). There, a Q dependence close to the law $\tau_w \propto Q^{-2}$ is found. Different possible scenarios for this crossover from Gaussian to non-Gaussian behavior were discussed in Ref. [2], in particular, the mode coupling theory [7–9] as well as a crossover from homogeneous to heterogeneous dynamics. The second interpretation might allow to rationalize apparently contradictory results from neutron scattering and relaxation techniques concerning the dynamical heterogeneous or homogeneous nature of the α relaxation (see, e.g., Refs. [5,10]).

While the simulations clearly demonstrate the crossover behavior, experimentally the evidence was limited. Certainly, whereas the mentioned crossover in the Q dependence found in the simulations is very encouraging, there was up to date no experimental evidence for it. Some deviations from Eq. (3) at high- Q values were reported for poly(vinyl methyl ether) (PVME) [11] and polyisobutylene [12]. A first clear evidence of such a crossover in polyisoprene has been reported by us in a recent paper [13]. In this extended paper, we explain in detail the experimental effort which has been necessary to achieve such a result. Moreover, we have also extended the previous MD simulations in PI to a wide temperature range above T_g .

For polymers, Q_{max} usually lies in the range $1.0 \leq Q \leq 1.5 \text{ \AA}^{-1}$ (see, e.g., Refs. [14–19]). Since standard high resolution quasielastic neutron scattering experiments typically cover a Q range $Q < 2 \text{ \AA}^{-1}$, the expected crossover is very difficult to access. High- Q values up to 5 \AA^{-1} at an energy resolution of 0.01 meV can be reached by the unique thermal neutron backscattering spectrometer IN13 at the Institut Laue-Langevin (ILL) in Grenoble. Even then, the experimental observation of the crossover found in the simulations is not an easy task. From an experimental point of view there are many difficulties. For instance, the full Q range from about 0.2 \AA^{-1} to 5 \AA^{-1} cannot be covered by one single spectrometer. Moreover, as a consequence of the strong Q dependence of $S_{self}(Q,t)$, it is very difficult to find a temperature for which the second relaxation step of

$S_{self}(Q,t)$ is well centered in both, the dynamical range and the total accessible Q range of all spectrometers. Finally, the amplitude of this second step is rather low in the high- Q regime (the prefactor $A(Q)$ [Eq. (2)] diminishes rapidly with increasing Q).

In order to achieve a wide coverage of the dynamical as well as the Q range we had to combine different types of instruments, two NSE spectrometers measuring in time and a thermal BS spectrometer measuring in energy. With the NSE spectrometers, we have covered the low- Q range $0.1 < Q < 1 \text{ \AA}^{-1}$. Since NSE allows deconvolution of the signal from the instrumental resolution function by simple division, the shape of the decay function [given by the value of the β parameter in Eq. (1)] can be determined with best accuracy. The IN13 BS spectrometer was used in order to extend our investigation towards the high- Q range (up to almost 5 \AA^{-1}).

In the simulations the crossover was established for the self-motion of the PI main chain protons. The protons located in the methyl groups show additional fast rotations [20,21], and therefore were not considered in the study of the α relaxation. In an analogous way, our experimental investigation has been focussed on the incoherent scattering from a PI sample with deuterated methyl groups (PI-d3). Due to the high value of the incoherent cross section of protons as compared to the other cross sections—incoherent as well as coherent—of the nuclei composing PI-d3, the scattered intensities are highly dominated by the H -self-motion contribution.

The paper is organized as follows. Section II deals with the experimental aspects, describing the sample, the neutron scattering techniques used, and the quantities studied with them. In Sec. III the obtained results are presented. The comparison with the simulation results is performed in Sec. IV, and the results are discussed in Sec. V where we elude to interpretations and implications of the findings. Finally, the conclusions are summarized.

II. EXPERIMENTAL

A. Sample

The polyisoprene sample was synthesized from isoprene monomers with deuterated methyl groups by anionic polymerization ($-\text{[CH}_2\text{—CH=C(CD}_3\text{)—CH}_2\text{]}_n-$). The molecular weight was determined by membrane osmometry to be $M_N = 108.000$. Size exclusion chromatography measurements yielded a polydispersity of $M_w/M_N = 1.03$. The microstructure of the sample consists of 6% 3,4 units, 69% cis 1,4 units, and 25% trans 1,4 units. Further details on the synthesis and characterization of the sample can be found in Ref. [19].

B. Neutron scattering

With exception of the neutron spin echo technique, an inelastic neutron scattering experiment measures the double differential cross section, i.e., the number of scattered neu-

trons in a solid angle $d\Omega$ which have experienced a change of energy $\hbar\omega$. It can be expressed as (see, e.g., Refs. [1,22,23]):

$$\frac{\partial^2 \sigma}{\partial \Omega \partial \omega} \propto \sum_{\alpha} (b_{inc}^{\alpha})^2 S_{self}^{\alpha}(Q, \omega) + \sum_{\alpha, \beta} b_{coh}^{\alpha} b_{coh}^{\beta} S_{pair}^{\alpha\beta}(Q, \omega). \quad (4)$$

b_{inc}^{α} and $b_{coh}^{\alpha(\beta)}$ refer to the incoherent and coherent scattering lengths of the isotope α (β) ($\alpha, \beta: \text{H, D, C, } \dots$) and relate to the interaction neutron with nucleus. Expression (4) contains two clearly distinguishable contributions: the incoherent (first term) and the coherent one (second term). The incoherent contribution involves the function $S_{self}^{\alpha}(Q, \omega)$, which is the Fourier transform of the self-correlation function of the positions of a nucleus of type α at different times, $G_s^{\alpha}(r, t)$,

$$G_s^{\alpha}(r, t) = \frac{1}{N_{\alpha}} \left\langle \sum_{i=1}^{N_{\alpha}} \delta(r - |\vec{r}_i^{\alpha}(t) - \vec{r}_i^{\alpha}(0)|) \right\rangle. \quad (5)$$

Here \vec{r}_i^{α} is the position of the atom i of type α and N_{α} the number of such nuclei in the sample. The brackets denote ensemble average.

For some simple cases—free nuclei in a gas, harmonic crystals, simple diffusion at long times— $G_s^{\alpha}(r, t)$ is a Gaussian function [22,23]; in an isotropic system this implies

$$G_s^{Gauss}(r, t) = \left[\frac{\alpha(t)}{\pi} \right]^{3/2} \exp[-\alpha(t)r^2]. \quad (6)$$

The calculation of the moments

$$\langle r^{2n} \rangle = \int_0^{\infty} r^{2n} G_s(r, t) 4\pi r^2 dr, \quad (7)$$

is then straightforward. For instance, the mean squared displacement of the atom $\langle r^2(t) \rangle$ in the Gaussian approximation is given by $\langle r^2(t) \rangle = 3/[2\alpha(t)]$. The intermediate scattering function then is entirely determined by $\langle r^2(t) \rangle$, given by

$$S_{self}^{Gauss}(Q, t) = \exp \left[-\frac{\langle r^2(t) \rangle}{6} Q^2 \right]. \quad (8)$$

In a general case, deviations of $G_s^{\alpha}(r, t)$ from the Gaussian form [Eq. (6)] may be expected. They may be quantified in a first approximation by the second-order non-Gaussian parameter α_2 defined as [24]

$$\alpha_2(t) = \frac{3}{5} \frac{\langle r^4(t) \rangle}{\langle r^2(t) \rangle^2} - 1, \quad (9)$$

which is, of course, null in the Gaussian case.

In the coherent part, $S_{pair}^{\alpha\beta}(Q, \omega)$ is the Fourier transform of the pair correlation function of the position of nuclei of types α and β , $G^{\alpha\beta}(r, t)$,

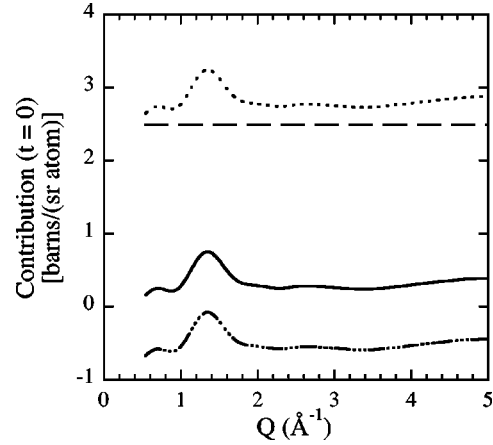


FIG. 1. Contributions to the scattering from Pid3: incoherent from the main chain protons I_{inc}^H (dashed line) and coherent I_{coh} (solid line) calculated from the simulations. The dotted line displays the addition of both, and corresponds to the total scattering (integrated over all frequencies) accessible by IN13. The dashed-dotted line is the result of subtracting $I_{inc}^H/3$ from I_{coh} , and gives the echo amplitude for the NSE measurements.

$$G^{\alpha\beta}(r, t) = \frac{1}{N_{\alpha} N_{\beta}} \left\langle \sum_{i=1}^{N_{\alpha}} \sum_{j=1}^{N_{\beta}} \delta(r - |\vec{r}_i^{\alpha}(t) - \vec{r}_j^{\beta}(0)|) \right\rangle. \quad (10)$$

These functions are also known as Van Hove correlation functions. It is straightforward to show that the static limit of the correlation function in Eq. (10) is the radial distribution function corresponding to isotopes α and β . The Fourier transform of this function to the Q space is the partial structure factor of the atom pairs α, β .

For the nuclei of our sample, the values of the scattering lengths are $b_{inc}^H = 25.274$ fm, $b_{inc}^D = 4.04$ fm, $b_{inc}^C = 0$, $b_{coh}^H = -3.7406$ fm, $b_{coh}^D = 6.671$ fm, and $b_{coh}^C = 6.6511$ fm [25]. From these values, the relative contributions from the different nuclei to the total scattering, either containing information on the self-motion or involving pair correlations with the same or another isotope, may be calculated. At first glance, due to the high value of b_{inc}^H as compared to the rest, the scattering from our Pid3 sample will be dominated by the incoherent contribution corresponding to the self-motion of the hydrogen nuclei in the main chain. The incoherent scattering from the three deuterons in the monomer (the carbons do not scatter incoherently at all) is negligible. The rest of the scattering comes from the pair correlations. The corresponding static contribution $I_{coh}(Q)$, the static structure factor measured by neutron scattering for Pid3, has been calculated from the simulations. It is shown in Fig. 1, together with the static incoherent contribution from the main chain protons I_{inc}^H . For this sample, the static coherent contribution displays a maximum centered at around 1.3 \AA^{-1} ; however, even in this Q range its value is much smaller than that of I_{inc}^H (about 1/3). As can be seen in the figure, the total scattering (dotted line) is slightly modulated by the structure factor $I_{coh}(Q)$.

Later, we will refer to earlier results on a fully deuterated sample PId8 [18]. Due to the nearly identical values of b_{coh}^D and b_{coh}^C the coherent scattering from a fully deuterated sample reveals the pair correlations of all the atoms in the sample with the same weight. In the static case, we will refer to this coherent contribution as the static structure factor $S(Q)$. In the investigated temperature range in polyisoprene, the value of Q_{max} signifying the first peak of $S(Q)$ is close to 1.3 \AA^{-1} [19,26]. We note that at this Q value also the static structure factor measured by neutron scattering for PId3 presents its first maximum (see Fig. 1).

1. IN13 backscattering spectrometer

Using neutrons with small wavelength λ ($\lambda \approx 2.23 \text{ \AA}$), the IN13 spectrometer at the ILL allows to access large values of the momentum transfer Q [$Q = 4\pi \sin(\theta/2)/\lambda$, with θ : scattering angle]. In order to achieve a high energy resolution δE , $\text{CaF}_2(422)$ crystals are used in exact or near backscattering at the analyzers and monochromator, resulting in $\delta E(\text{HWHM}) \approx 5 \text{ \mu eV}$, where HWHM stands for half width at half maximum. The energy of the incident neutrons is scanned by heating or cooling the monochromator at a fixed Bragg angle. The experiments were performed varying the incident neutron energy at 0.3 \mu eV/min . An energy transfer interval of $-130 \text{ \mu eV} \leq \hbar\omega \leq 100 \text{ \mu eV}$ was explored.

Seven spherically curved composite crystal analyzers, each covering a large solid angle of 0.18 sr (total angular range: $24.4^\circ < \theta < 155.9^\circ$) allow the energy analysis of the scattered neutrons. These are counted by a multidetector array of 32 ^3He tubes. An additional small angle region, giving unreliable count rates, could not be used. The Q range at very high- Q values had to be restricted slightly due to contamination from aluminum Bragg peaks. The reliable Q range was limited to $1.2 \leq Q \leq 4.7 \text{ \AA}^{-1}$. There, the spectra have been grouped into nine groups which were chosen to be approximately equidistant in the $\ln(Q)$ scale. The sample (thickness: 0.26 mm) was filled in a flat Al container and placed at 135° with respect to the incident beam. The measurements were performed at 260 K (measuring time: 2 days), 280 K (3 days) and 300 K (2.5 days). The instrumental resolution function was determined from the scattering of the sample at 1.5 K. Initial data treatment was carried out correcting for effects of detector efficiencies, scattering from sample container, and instrumental background. Multiple scattering effects were ignored since they become relatively weak in this high- Q range and the transmission of the sample was quite high (see below).

2. Neutron spin echo spectrometers

NSE is the neutron scattering technique offering the highest energy resolution. For each neutron individually the energy transfer in the scattering process is coded into its spin rotation [27]. Applying precession magnetic fields before and after the scattering event, the polarization of the neutron depends only on the velocity difference of each neutron individually, irrespective of its initial velocity.

As a singular feature of NSE, it accesses the scattering functions in the time domain, i.e., the intermediate scattering

functions. These are the spatially Fourier transforms of the correlation functions in Eqs. (5) and (10). NSE measures a normalized function [27]:

$$\tilde{S}_{NSE}(Q,t) = \frac{I_{coh}\tilde{S}_{pair}(Q,t) - \frac{1}{3}I_{inc}\tilde{S}_{self}(Q,t)}{I_{coh} - \frac{1}{3}I_{inc}}, \quad (11)$$

where $\tilde{S}_{pair}(Q,t)$ and $\tilde{S}_{self}(Q,t)$ are the normalized intermediate pair and self-correlation functions (they are normalized to their value at $t=0$). I_{coh} and I_{inc} denote again the coherent and incoherent intensities. The static value of the NSE signal is given by the denominator in Eq. (11). For our PId3 sample, it is shown as the dashed-dotted line in Fig. 1. The signal at low Q is dominated by the incoherent scattering. The NSE experiment then directly measures $\tilde{S}_{self}(Q,t)$, related to the self-motion of the hydrogens in the main chain. The time variable depends on the precession field B , the wavelength λ , and the length of the precession field L : $t \sim BL\lambda^3$.

In this work, we present results obtained by the two NSE instruments: the multidetector NSE instrument IN11C at the ILL in Grenoble and the Jülich NSE spectrometer at the FRJ-2 reactor in Jülich. At IN11C $\lambda = 5.54 \text{ \AA}$ was used. The multidetector at this instrument covers an angular range of 30° in the horizontal plane. It was placed at 32° , 65° , and 85° scattering angle for its central detector. Thereby, a Q range $0.34 \leq Q \leq 1.68 \text{ \AA}^{-1}$ and a time range $8.4 \text{ ps} \leq t \leq 1.4 \text{ ns}$ were explored. Measurements were performed at 300 K, 320 K, and 340 K. Typical measuring times were 10 h. In the 65° and 85° positions also 280 K was investigated, though with poorer statistics. A perpendicular transmission of 0.82 was measured for this wavelength. At the Jülich NSE spectrometer, we used $\lambda = 8 \text{ \AA}$. A time interval of $100 \text{ ps} \leq t \leq 22 \text{ ns}$ was covered. With this instrument, we focussed the study on the low- Q region. In order to observe a meaningful decay of the correlation function in the NSE time window, a high enough temperature was chosen (340 K). Four Q values were investigated: 0.1, 0.15, 0.2, and 0.3 \AA^{-1} , using measuring times between 24 and 32 h per Q value. For each momentum transfer the instrumental resolution function was determined from the elastic scattering of the sample at 10 K (IN11C) and from measurements on a carbon powder sample (Jülich NSE). The instrumental background from the cryofour and the Al container was measured separately for each Q (with measuring times similar to those for the measurements on the sample, i.e., 24 h for the Jülich NSE spectrometer). It was thereafter subtracted from the experimental spectra using the appropriate transmission factors. The background corrected spectra were divided by the resolution function revealing the normalized intermediate dynamic structure factor.

III. RESULTS

Figure 2 shows some of the spectra obtained by IN13 at 280 K and different Q values. As explained in Sec. II B, they mainly display the incoherent scattering function of the protons. The spectra are compared with the instrumental resolu-

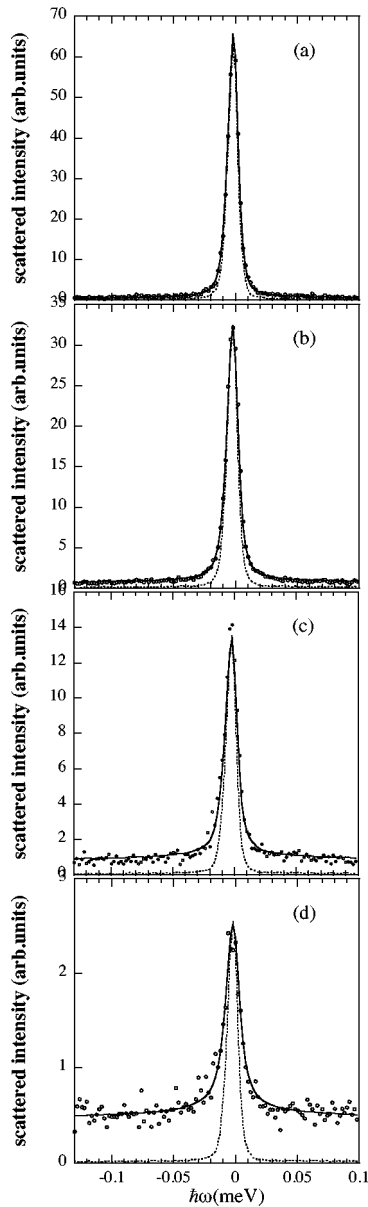


FIG. 2. IN13 spectra obtained for PId3 at 280 K and different Q values: 1.2 \AA^{-1} (a), 1.9 \AA^{-1} (b), 2.9 \AA^{-1} (c), and 4.7 \AA^{-1} (d). The dotted lines show the instrumental resolution function obtained at 1.5 K; the solid lines are fits to the Fourier transform of KWW functions ($\beta=0.40$) plus a Q -dependent flat contribution.

tion. The spectra display significant broadenings with increasing Q . The broadened spectra reveal dynamical processes—in this case the α relaxation—with time scales within the dynamical range of the instrument. Faster mobilities translate to broader spectra. We also note a dramatic drop of the spectral intensity: the ratio between the maxima at 1.2 and 4.7 \AA^{-1} (the lowest and the highest Q accessed by IN13) is around 20. As outlined in Sec. I, the lowering of the α -relaxation amplitude is caused by faster motional processes. These include the vibrations and the fast dynamics characteristic for glass-forming polymers (boson peak, fast process, . . .) which are observed at higher frequencies [28]. Another signature of these fast dynamics is the presence of a

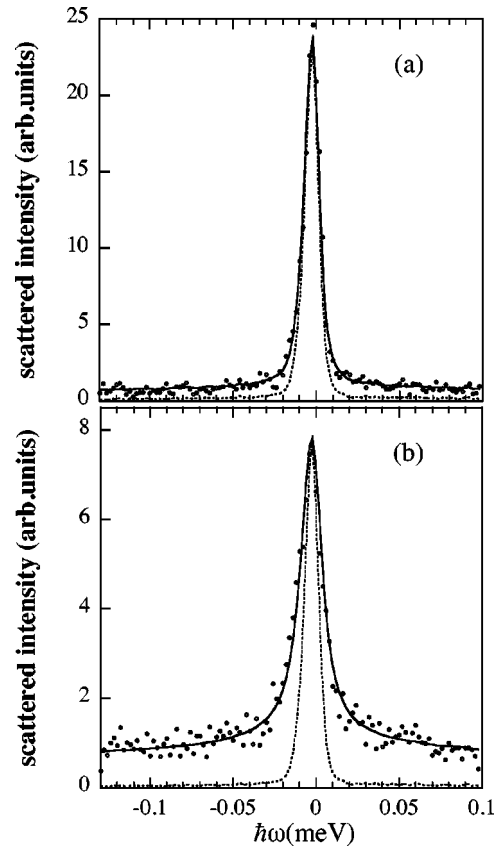


FIG. 3. IN13 spectra obtained for PId3 at 2.9 \AA^{-1} at 260 K (a) and 300 K (b). Lines as in Fig. 2 ($\beta=0.40$ for 260 K, $\beta=0.50$ for 300 K).

flat contribution in the spectra which becomes relatively important at high Q [see Figs. 2(c) and 2(d)].

An increasing broadening is also observed in the spectra at a given Q value when the temperature increases. For an intermediate value of Q this is shown in Fig. 3 for the highest and the lowest temperatures investigated (300 and 260 K); the corresponding spectrum at 280 K is displayed in Fig. 2(c). The dynamical process causing the quasielastic intensity becomes thus faster with increasing temperature.

A direct observation of the decaying self-correlation function in the time domain is possible with NSE. For different Q values, Figs. 4 and 5 display the temporal evolution of the intermediate incoherent scattering function at 320 K and 340 K, respectively. The high quality of these data is remarkable. However, we emphasize the difficulties of a measurement of the self-motion by NSE at partially deuterated samples. The IN11C measurements were extended up to $Q=1.68 \text{ \AA}^{-1}$. Nevertheless, only in the Q range $Q \leq 1.0 \text{ \AA}^{-1}$ it was possible to obtain useful information. Due to partial cancellation [Eq. (11)] the NSE amplitude decreases strongly, if the coherent contribution assumes nonnegligible values. Approaching to the Q range where $I_{coh}(Q)$ shows its first peak ($\approx 1.3 \text{ \AA}^{-1}$) the NSE signal almost vanishes (see Fig. 1). The NSE study is thus restricted to $Q \leq 1.0 \text{ \AA}^{-1}$.

As can be seen in Figs. 4 and 5, the spectra decay faster with increasing Q and temperature. Moreover, from simple inspection of the curves it becomes clear that the shape of the

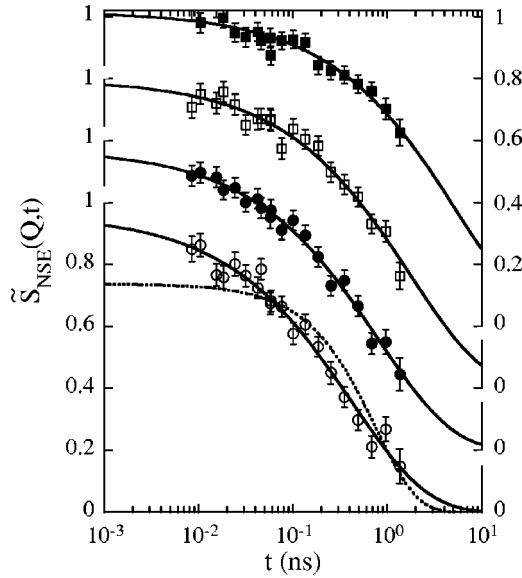


FIG. 4. IN11C results for PID3 at 320 K and different Q values: 0.45, 0.60, 0.74, and 0.88 \AA^{-1} (top to bottom). Solid lines correspond to KWW descriptions with $\beta=0.55$. The dotted line shows a single exponential function for comparison.

decays is much more stretched than a single exponential function (see the example depicted in Fig. 4).

The results were analyzed in terms of KWW functions [Eq. (1)], which are well known to describe the relaxation function and the decay of the density fluctuations in glass-forming liquids (see, e.g., Ref. [29]). As backscattering techniques measure in the frequency domain, for the IN13 spectra the Fourier transform of the KWW function was used.

As first ingredient, a KWW analysis requires the determination of the stretching parameter β . Due to the convolution problems this is hardly feasible on the basis of the BS data.

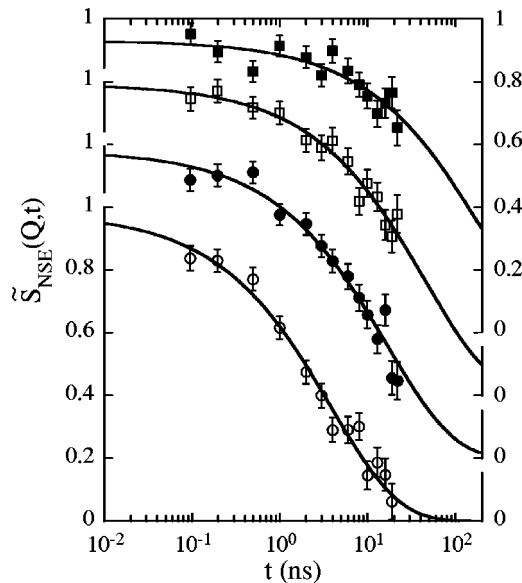


FIG. 5. Jülich NSE results for PID3 at 340 K and different Q values: 0.10, 0.15, 0.20, and 0.30 \AA^{-1} (top to bottom). Lines correspond to KWW descriptions with $\beta=0.57$.

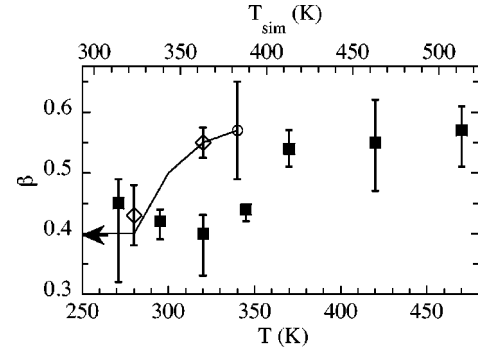


FIG. 6. Temperature dependence of the β parameter as obtained from the NSE experiments on PID3 (\circ) and PID8 (\diamond), and from the simulations (\blacksquare). The arrow marks the value determined for this parameter from dielectric spectroscopy [18]. The values fixed for the analysis of the neutron scattering results in this work are shown by the solid line.

At 340 K, the high quality of the Jülich NSE data (Fig. 5) allows for an independent fit revealing $\beta=0.57\pm 0.08$. Figure 6 shows a compilation of the values obtained for the β parameter from different experiments—this work, dielectric spectroscopy and NSE on PID8 [18]. A tendency to increase with T is observed for β . On the basis of the experimental results at hand, for the further evaluation we interpolated β to the values shown in Fig. 6 as a solid line and kept it fixed.

The description of the IN13 curves in terms of the Fourier transform of Eq. (1) with fixed shape parameters is very satisfactory. This may be seen in Figs. 2 and 3. A flat contribution was also allowed in the fitting procedure. For the three temperatures investigated the characteristic times are displayed as a function of Q in Fig. 7. A strong decrease of τ_w with increasing Q takes place. We note that at 280 K the uncertainties in the determination of τ_w are smaller than at the other temperatures, since there the dynamical process occurs at time scales well accessible for IN13 in the whole Q

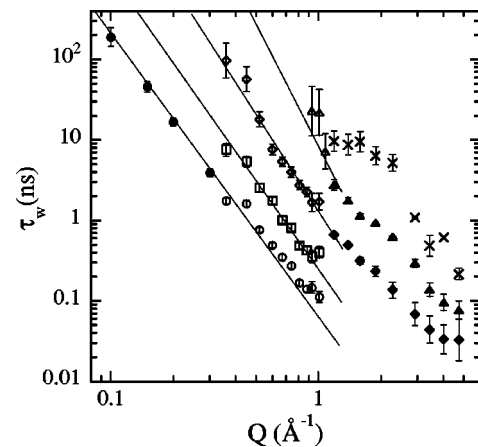


FIG. 7. Momentum transfer dependence of the characteristic times obtained from the KWW description of the results on PID3 obtained by IN13 (\times , 260 K; \blacktriangle , 280 K; \blacklozenge , 300 K), IN11C (\triangle , 280 K; \diamond , 300 K; \square , 320 K; \circ , 340 K), and Jülich NSE spectrometer (\bullet , 340 K). Solid lines show an orientative law $Q^{-2/\beta}$ corresponding to each temperature for $T\geq 280$ K.

range. At 260 K the dynamics becomes slower and, due to the rather strong Q dependence of τ_w , the broadenings in the low- Q spectra are very small. Contrarily, for the highest temperature (300 K) the dynamics can be well followed in the low- Q range, where nice broadenings associated to relatively fast dynamics are detectable, but the decay of the overall intensity is stronger and leads to very weak signals at high- Q values. In fact, the amplitude A for the α relaxation can be well described by means of Eq. (2). The values for the mean squared displacement $\langle u^2 \rangle$ associated with the fast process are $0.43 \pm 0.02 \text{ \AA}^2$ at 260 K, $0.55 \pm 0.02 \text{ \AA}^2$ at 280 K, and $0.58 \pm 0.01 \text{ \AA}^2$ at 300 K, in good agreement with previous BS results on a similar sample [5,30].

Also for the NSE spectra the KWW function offers a good description (see Figs. 4 and 5). The resulting characteristic times from the fitting procedure are plotted in Fig. 7 together with those deduced from the IN13 measurements. It is noteworthy that at 300 K a very wide Q range ($0.34 \leq Q \leq 4.7 \text{ \AA}^{-1}$) has been covered by the combination of IN13 and IN11C measurements; in this Q range, the time scales spread over almost four decades. Though unfortunately no overlap in Q of the results from the two techniques was possible due to the problems commented above, the Q dependence of τ_w is very well defined in the full range for this temperature. It is important to note that the extrapolated behavior from the low- Q side (solid line) perfectly matches the lowest Q result of IN13. We emphasize again the experimental difficulties and the importance to select properly the temperature range in order to achieve meaningful results over such a large dynamic range. At 280 K the dynamics becomes already too slow to be well characterized in the low- Q range. The Q dependence in this range has nevertheless been perfectly determined for 340 K by combining the results of the two NSE machines. For this temperature, the full decade $0.1 \leq Q \leq 1 \text{ \AA}^{-1}$ has been covered.

With these results at hand, one may first scrutinize the Gaussian character of the self-correlation function. In Fig. 7, we have compared the Q -dependent characteristic times with the Gaussian prediction [Eq. (3)], represented by the solid lines. As the value of the β -parameter slightly increases with temperature, the slopes of the power laws predicted by the Gaussian approximation decrease in absolute value towards higher temperatures. Figure 7 shows that Eq. (3) describes very well the Q dependence of the experimentally determined characteristic times in the range $Q \leq 1 \text{ \AA}^{-1}$ for $T \geq 300 \text{ K}$ and is well compatible with the results at 280 K within the experimental uncertainties. However, above 1 \AA^{-1} the times deviate from such law to follow a weaker Q dependence.

In Fig. 8(a), we have replotted the characteristic times of Fig. 7 exponentiated to the power of β . Considering Eq. (3), in this representation all the results reflecting Gaussian behavior should show the same slope ($\tau_w)^\beta \propto Q^{-2}$ (solid lines). Again the goodness of the Gaussian approximation for the self-correlation function at $Q \leq 1 \text{ \AA}^{-1}$ becomes evident. The use of $(\tau_w)^\beta$ has the advantage that the influence of the temperature on the Q dependence through the change in β is removed. Starting from Fig. 8(a), we can now condense all the available information from the different temperatures in-

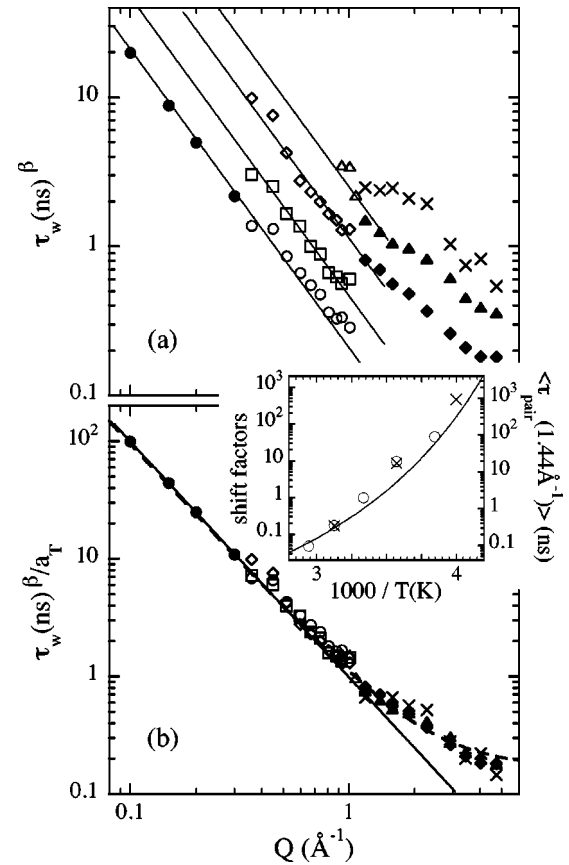


FIG. 8. (a): Momentum transfer dependence of the characteristic times in Fig. 7 exponentiated to the power of β . (b) Master curve constructed shifting the points in (a) by the appropriate factors a_T . Straight lines show a Q^{-2} dependence. The dashed line shows the description of the master in terms of an anomalous jump diffusion model [Eq. (17)] with $\ell_0 = 0.42 \text{ \AA}$. The inset compares the shift factors obtained from dielectric spectroscopy (solid line) and from this neutron scattering study on PId3 (O) (see the text). The average times from the pair correlation function measured by IN11 at 1.44 \AA^{-1} on PId8 are also displayed (\times).

vestigated by constructing a master curve. In this procedure, the temperature dependence is removed applying shift factors a_T to the results obtained at the different temperatures. Choosing a reference temperature T_R , $(\tau_w)^\beta / a_T$ should collapse on the data corresponding to T_R . Figure 8(b) results from such a procedure with $T_R = 300 \text{ K}$. Within the experimental uncertainties, the coincidence of the results obtained at the different temperatures is nearly perfect. A Q^{-2} dependence of $(\tau_w)^\beta$ is obtained at low Q crossing over to a weaker power law at around $Q \approx 1.3 \text{ \AA}^{-1}$. Thus, we have experimentally established a crossover from Gaussian to non-Gaussian character of the α relaxation similar to that reported for the simulated sample.

Before coming to the discussion, let us now investigate how the shift factors used for building the master curve compare with other results on the temperature dependence of PI. For example, we can compare them with those obtained by dielectric spectroscopy. When the shape of the correlation function changes with temperature, it is meaningful to present the results on the thermal evolution of the character-

istic time scale in terms of the average time $\langle \tau \rangle$. $\langle \tau \rangle$ is the first moment of the equivalent distribution of single exponentials. In the case of KWW functions, $\langle \tau \rangle$ is given as

$$\langle \tau \rangle = \frac{\Gamma\left(\frac{1}{\beta}\right)}{\beta} \tau_w, \quad (12)$$

where Γ is the Gamma function. $\langle \tau \rangle$ observed by spectroscopic techniques often matches the $\langle \tau_{self}(Q) \rangle$ obtained from the self-correlation function at $Q \approx 1 \text{ \AA}^{-1}$ [31]. In the particular case of PI, it has been found that this occurs for $Q = 0.9 \text{ \AA}^{-1}$ [30]. The inset of Fig. 8 compares the shift factors obtained by dielectric spectroscopy [32,33] (solid line) with those for $\langle \tau_{self}(Q = 0.9 \text{ \AA}^{-1}) \rangle$ (crosses). In both cases $T_R = 300 \text{ K}$. In this inset, we have also displayed the IN11 results on the average time of the pair correlation function at 1.44 \AA^{-1} [18]. The agreement between the three sets of data is very good.

IV. DETAILED COMPARISON WITH SIMULATION

In Sec. III, we have established the crossover from a Gaussian to a non-Gaussian character of the self-correlation function measured on the PI₃ sample. Such a crossover takes place at $Q \approx 1.3 \text{ \AA}^{-1}$, a value close to Q_{max} . This is just the result from the simulations on PI we wanted to validate. Now we would like to stress the direct comparison between simulation and experimental results. How do the absolute values of the characteristic times compare? Is the shape of the decay similar in both cases, etc.?

To answer these questions, at equivalent Q values we directly compare the intermediate scattering functions obtained from the NSE measurements with those from the simulations at 363 K [2]. We find closest agreement between both datasets for a temperature of about 320 K for the real sample. For $Q = 0.67 \text{ \AA}^{-1}$, Fig. 9(a) shows the experimental self-correlation function of the main chain protons at 320 K (points) and that obtained from their trajectories in the simulations at 363 K (line). Both decays take place in a very similar way. We note that the amplitude of the experimental data is higher than that of the simulation results. The comparison in the figure has been done reducing the experimental scale by 17% with respect to the simulation scale (see the corresponding axis in the figure). The need of such an adjustment can be rationalized taking into account how the NSE data are normalized. As a result of the polarization analysis after the scattering process, a NSE spectrometer offers only a limited band pass to the scattered neutrons. Inelastically scattered neutrons with wavelengths λ shorter than those that the bandpass allows, are not transmitted through the instrument and do not participate in the normalization [denominator of Eq. (11)]. The value determined by the NSE instrument for the static signal is therefore underestimated. An exact calculation of the error in the experimental normalization is not straightforward since a complete knowledge of the scattering functions and the bandpass frequency range is required. We note that the NSE signal includes both, the incoherent and the partial coherent structure factors as

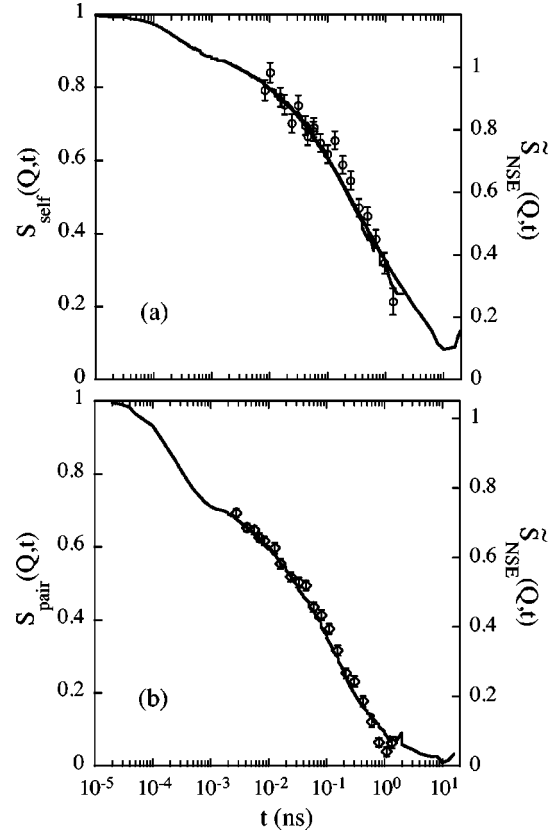


FIG. 9. Direct comparison between simulation and experimental results. In (a) the self-correlation function calculated from the main chain proton trajectories at 0.7 \AA^{-1} and 363 K (line) is displayed together with the IN11C results on the PI₃ sample at 0.67 \AA^{-1} and 320 K (\circ). In (b) the pair correlation function calculated from simulations at 1.45 \AA^{-1} and 363 K (line) and the IN11 result for PI₈ [18] at 1.44 \AA^{-1} and 320 K (\diamond) are presented.

mixed in the polarization analysis; in the case of partially deuterated samples, the situation might be quite complicated (see, e.g., Ref. [26]) and the experimental result can be very much influenced, e.g., by a slightly deficient deuteration. The matching factor has therefore been adjusted though its need is clearly justified.

Even if this paper is focused on the self-motion of the main chain protons in PI, in order to further check the validity of the simulations we can compare experimental and simulation results on another correlation function for which experimental data are available: the coherent scattering function or dynamic structure factor measured from a fully deuterated sample PI₈ [18]. Giving additional support to the simulations, Fig. 9(b) shows that for $Q = 1.44 \text{ \AA}^{-1}$ the pair correlation function measured on PI₈ at 320 K [18] superimposes with high accuracy with its simulated counterpart at 363 K. Again the NSE amplitude has been adjusted to match the simulated data. We note that the wavelength used in that NSE measurements was shorter ($\lambda = 4.68 \text{ \AA}$), leading to a more accurate normalization of the data. Simulations and experimental results are thus approximately equivalent if a shift in the temperature scale of about 40 K is assumed. Then the time scale as well as the shape of the decays are similar. Such a temperature shift was also reported for MD simula-

tions of a model of a low-molecular glass-forming system: orthoterphenyl [34]. In our case the shift might be due to several reasons. For instance, to the difference in the microstructure of the samples—the simulated chain consists of 18% cis units and 82% trans units. Also different tacticities could lead to some differences in the dynamics. Another origin could be that the force field used in the simulations [35] was not perfectly calibrated. The potentials involved in the simulations are from both intermacromolecular and intramacromolecular nature. It has been recently shown by Smith *et al.* [36] that the time scale of the α relaxation resulting from the MD simulations in polybutadiene is quite sensitive to slight changes of the local intrachain potentials. Thus, a refinement of the rotational potentials based on the comparison with experiments could possibly result in a more realistic force field for PI.

The overall corrections of the simulations may be tested further in looking at the temperature dependent relaxation dynamics. For this purpose new MD simulations have been run at temperatures ranging from 314 K to 513 K. The data were analyzed in the same way as reported in Ref. [2] and above, and reveal information on the shape as well as on the characteristic time. We first discuss the results on the shape of the relaxation. Contrary to what is usually assumed (e.g., also for fully deuterated PI [18]), in this experimental study we have found deviations from the time-temperature superposition principle in PI. The β -value increases from $\beta \approx 0.40$ at $T \leq 280$ K (dielectric data, pair correlation function close to the first peak) to $\beta \approx 0.57$ at 340 K (see Fig. 6). A similar trend can also be deduced from the simulations. Together with the experimental results on the β parameter, Figure 6 presents those obtained from a fit of the self-correlation function of the main chain protons calculated from the simulations using Eq. (1). The best estimates for the β values are shown as solid squares. The bars in these points indicate the range within which the value of the β parameter varies in the Q -region investigated ($0.2 \leq Q \leq 5 \text{ \AA}^{-1}$). In the temperature range under study, also an increase from $\beta \approx 0.40$ to $\beta \approx 0.60$ can be observed. In the comparison made in Fig. 6, we have taken into account the shift of around 40 K found from the direct comparison of the spectra (Fig. 9), by shifting the temperature scale of the simulation (above) with respect to the scale for the sample temperature (below). Though qualitatively the behavior of β agrees for experiments and simulation, we note that the experimental β value at 320 K is larger than that obtained from a fit of the simulated spectra at the corresponding temperature $T = 363$ K. The change in shape appears at somewhat higher temperature in the simulations compared to the experiment.

Figure 10 displays the observed temperature dependencies of the relaxation times. In order to make characteristic times of relaxation spectra of changing shape comparable, we present the average times [Eq. (12)]. The full squares are the simulation results, the open circles the neutron data, and the solid line the temperature dependence predicted on the basis of dielectric measurements on the same sample [32,33]. Again the simulation results were shifted in temperature by 43 K. The agreement between all data sets is very satisfactory and again nicely validates the simulation.

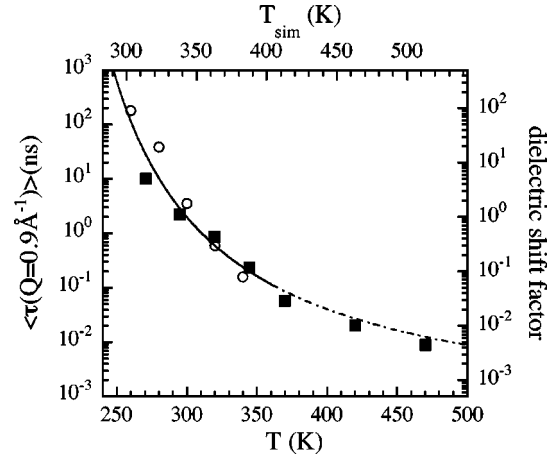


FIG. 10. Temperature dependence of the average time obtained from the experiments (\circ) and from the MD-simulations (\blacksquare) for $Q = 0.9 \text{ \AA}^{-1}$. The solid line shows the temperature dependence observed from the dielectric spectroscopy. Its extrapolation to temperatures higher than those experimentally accessed is represented by the dashed-dotted line.

We finally compare the Q dependence of the characteristic time as obtained from experiment and simulations. For a direct comparison, we note that the experimental results are affected by the coherent scattering contribution in the high- Q range. From inspection of Fig. 1, the $Q \leq 1 \text{ \AA}^{-1}$ results should not be influenced by coherent scattering, while the lower- Q part of the IN13 data should contain an appreciable coherent contribution [the peak of $I_{coh}(Q)$ is between 1 and 2 \AA^{-1} , see Fig. 1]. The easiest way for a direct comparison is to take advantage of the knowledge on all the atomic trajectories from the MD simulations and to build the total scattering function for the PID3 sample considering the different contributions [see Eq. (4)]. As an example in Fig. 11(a), we show the coherent and the incoherent contributions obtained from the simulations at $Q = 1.3 \text{ \AA}^{-1}$, i.e., where the coherent contribution is maximal. These functions are weighted by the corresponding static amplitudes I_{coh} and I_{inc} . As can also be seen in Fig. 1, the ratio between them is about 1:3. If the characteristic times for both decay functions were the same, then the time scale of the resulting total function would not be affected. However, a fit with Eq. (1) and $\beta = 0.40$ fixed to the slow decays of the pair and the self-functions gives a significantly longer time for the coherent contribution (136 ps compared to 54 ps). This is a consequence of the deGennes-type narrowing found in glass-forming systems for the α relaxation [12]. The resulting characteristic time for the total function is 70 ps, somewhat longer than the 54 ps found for the self-motion of the main chain protons. The fit of both, the incoherent and the total decay leads to the values for the characteristic times shown in Fig. 11(b). As expected, they coincide below 1 \AA^{-1} , but a slight modulation mirroring $I_{coh}(Q)$ can be found in the case of the total scattering. Due to the small amplitudes of the second decay, above 3 \AA^{-1} the uncertainties in the determination of the time scale are higher. We note, moreover, that the calculations involving coherent contributions extend only down to 0.5 \AA^{-1} . The dimensions of the simulated cell do not allow

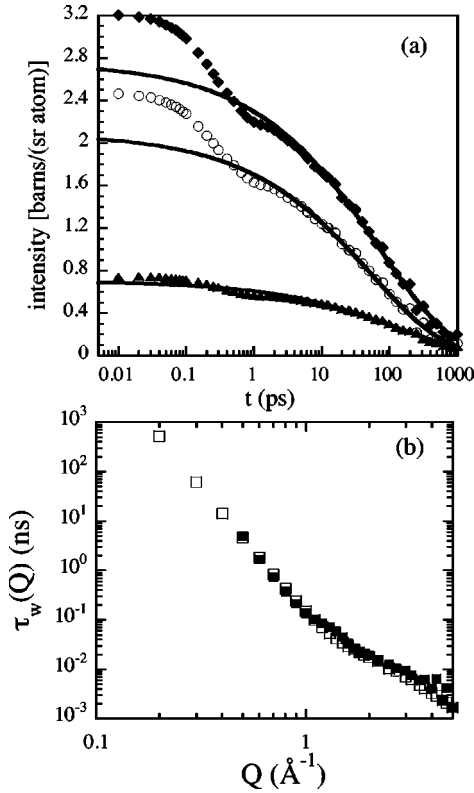


FIG. 11. Influence of coherent scattering on the results at $Q = 1.3 \text{ \AA}^{-1}$ (a) Contributions of the self-motion of the main chain protons (\circ) and of the pair correlation of the Pid3 sample (\blacktriangle) obtained from the MD simulations. The total function is also displayed (\blacklozenge). Solid lines show the description of the self-contribution and the total scattering function by KWW functions with $\beta=0.40$. (b) Comparison between the characteristic times obtained from the simulations when considering the self-contribution of the main chain protons (\square) and the total scattering function for the Pid3 sample (\blacksquare).

to calculate the pair correlation functions beyond such a limit. However, we should expect indistinguishable time scales with and without considering the coherent contribution in the low- Q regime.

The comparison between experiments and simulation is performed in Fig. 12. By applying a shift factor a_T to the values of $(\tau_w)^\beta$ obtained from the simulations for the total scattering function, we have superimposed them to the master plot previously built from the experimental results (Fig. 8). Considering that at the highest Q points the determined times are subject of some uncertainties, the agreement between both sets of data is extremely good. In this figure, we have also included the experimentally determined static structure factor at 314 K [19]. In this way, it can be clearly seen that the crossover takes place in the neighborhood of Q_{max} . We thus conclude that the crossover found in the simulations takes place in a similar way in the real sample. Apart from the shift in temperature (corroborated by the a_T used for matching the points in the master curve), a quantitative equivalence is found between experiment and simulations.

Inspecting the new temperature dependent simulations we

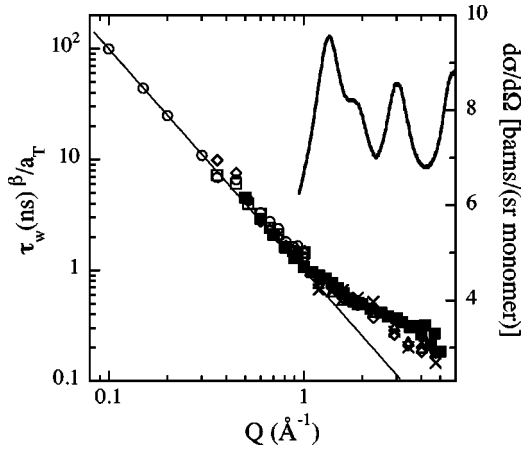


FIG. 12. Master curve built by combining experimental (empty symbols) and simulation (\blacksquare) results on the Pid3 sample. The straight line shows a Q^{-2} dependence. The static structure factor determined by D20 on Pid8 at 314 K [19] is displayed for comparison (solid line). The corresponding scale is shown starting from the level estimated for the incoherent scattering contribution.

may also ask, whether the crossover between Gaussian and non-Gaussian self-correlation functions depends on temperature. For that purpose, using temperature dependent shift factors, in Fig. 13, we display the simulated Q -dependent relaxation times again in form of a master plot. As may be seen, the data from all temperatures collapse to a single master curve. Thus, the crossover to non-Gaussianity is not affected by temperature, but appears to be an intrinsic property of the sublinear diffusion process.

Finally, the deviations from Gaussianity reflected in the Q dependence of the characteristic time at high- Q values should be associated to nonvanishing values of the $\alpha_2(t)$ parameter. This is demonstrated in Fig. 14, where the values for $\alpha_2(t)$ computed from the MD simulations according to Eqs. (9) and (7) are displayed. This parameter shows two

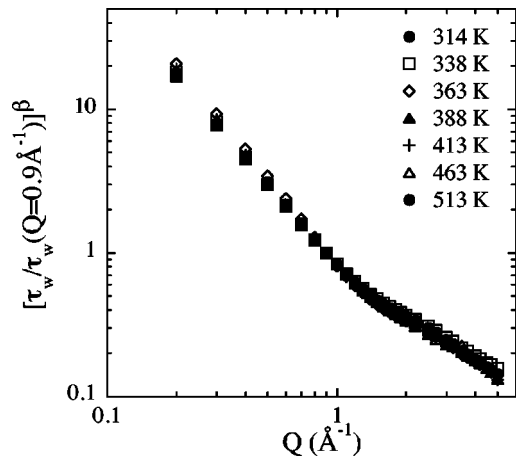


FIG. 13. Master curve obtained from the MD-simulation results by dividing the characteristic times corresponding to a given temperature by the value at 0.9 \AA^{-1} and exponentiating them to the proper β value. The different symbols correspond to the different temperatures indicated.

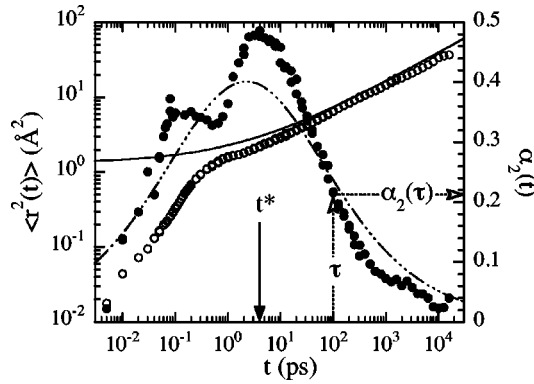


FIG. 14. Time evolution of the mean squared displacement $\langle r^2 \rangle$ (○) and the non-Gaussian parameter α_2 (●) obtained from the simulations at 363 K for the main chain protons. The solid vertical arrow indicates the position of the maximum of α_2 , t^* . At times $\tau > \tau(Q_{max})$, the crossover time, α_2 assumes small values, as in the example shown by the dotted arrows. The corresponding functions $\langle r^2 \rangle$ and α_2 deduced from the analysis of the experimental data at 320 K in terms of the jump anomalous diffusion model are displayed as lines: solid for $\langle r^2 \rangle$ and dashed dotted for α_2 .

maxima, the first of which can be attributed to the particular microscopic dynamics, which is mainly determined by the relative motion of the protons with respect to the main chain carbons [2]. The second peak, centered at $t^* \sim 4$ ps, relates to the onset of sublinear diffusion which shows itself in the mean squared displacement obtained from the simulations. It is responsible for the deviations found from Gaussian behavior at high- Q values. This can easily be realized with the following argument. At low Q , below 1.3 \AA^{-1} , the characteristic time τ_w is slow, $\tau_w(Q \leq 1 \text{ \AA}^{-1}) \geq 100$ ps [see Fig. 11(b)]. As can be deduced from Fig. 14, the value of the non-Gaussian parameter corresponding to $t \geq 100$ ps is quite small, i.e., $\alpha_2[\tau_w(Q \leq 1 \text{ \AA}^{-1})] \leq 0.2$. However, above the crossover Q value, the characteristic time becomes fast, with values below 10 ps for $Q \geq 2 \text{ \AA}^{-1}$. These times correspond just to the region where $\alpha_2(t)$ presents its second maximum, i.e., they are close to t^* . Thus, we can see that the deviations towards non-Gaussian behavior of τ_w are intimately linked to the main peak of $\alpha_2(t)$ and therefore their origin should be common.

V. INTERPRETATION AND DISCUSSION

Any theoretical approach or model considered for interpreting the crossover found in the Q dependence of $\tau_w(Q)$ should also reproduce the behavior of $\alpha_2(t)$. Several scenarios may be invoked [2]. (i) For instance, the mode coupling theory (MCT) for the glass transition [7–9] predicts a Q dependence for the characteristic time of the self-correlation function that at high- Q values strongly deviates from that expected in the Gaussian case. Qualitative agreement between the MCT predictions and the simulated $\tau_w(Q)$ is found [2]. Moreover, $\alpha_2(t)$ calculated in the framework of the MCT for a hard-sphere system also shows a qualitatively similar behavior to that reported here. (ii) Most physical pictures given for the rationalization of α_2 are based on the

existence of the so-called “mobile particles” or on considerations related to the ill-defined concept of dynamical heterogeneity [10]. A possible scenario based on the widely assumed idea of identifying Gaussian behavior with dynamically homogeneous behavior was already discussed in Ref. [2]. In such a scenario, the crossover could be understood as a homogeneous to heterogeneous crossover of the incoherent dynamics involved in the α relaxation. As it was mentioned in Ref. [2], this interpretation would imply that the results obtained by different techniques could be affected by the underlying dynamic heterogeneity at t^* in a different way. The closer the time scale of the α process probed by a particular technique is to the t^* range, the more sensible this technique is to the heterogeneous dynamics. On the other hand, it is noteworthy that in most of the works invoking the concept of dynamical heterogeneity the origin of the nonvanishing values of α_2 is usually sought in connection with the origin of the nonexponential behavior of the α relaxation, i.e., the stretching of the relaxation function. In none of these works the Q dependence of the characteristic relaxation time is considered.

Here, we will focus on another explanation of the crossover which was recently pointed out [13]. It bases on the existence of a distribution of discrete jumps underlying the atomic motions in the α process. As we will see, this simple interpretation, which, in principle, is compatible with the framework of the MCT, gives account for the observed behavior in PI and allows to deduce all the universal features reported up to date for the non-Gaussian parameter α_2 in different glass-forming systems.

The result which is now established beyond doubt is the law $\tau_w \propto Q^{-2/\beta}$ [Eq. (3)] at $Q < Q_{max}$ and its consequence: the sublinear diffusion process for the atomic motions in that Q range. We have also shown a clear correlation between the non-Gaussian parameter α_2 and the deviations from Gaussian behavior found for $\tau_w(Q)$. We now like to dwell on these results, in order to understand the crossover. It is well known that in the simple jump diffusion model, proposed a long time ago (see Refs. [23,37,38]), finite jump lengths tend to cause a bending of the dispersion for the diffusive relaxation time away from the Q^{-2} law which takes place for simple diffusion at low Q . The jump diffusion model [23,37,38] assumes that an atom remains in a given site for a time τ_0 , where it vibrates around a center of equilibrium. After τ_0 , it moves rapidly to a new position separated by the vector $\vec{\ell}$ from its original site. For simple diffusion (SD) the incoherent intermediate scattering function is

$$S_{self}^{jump,SD}(Q,t) = \exp\left[-b(Q)\frac{t}{\tau_0}\right], \quad (13)$$

where $b(Q)$ depends on the particular geometry of the jumps involved, i.e., on the vectors $\vec{\ell}$. A reasonable assumption for liquids and disordered systems is that they are randomly oriented and that their moduli are distributed according to a function

$$f_0(\ell) = \frac{\ell}{\ell_0^2} \exp\left(-\frac{\ell}{\ell_0}\right), \quad (14)$$

which involves a preferred jump distance ℓ_0 . The average value of the jump length is then $\langle \ell \rangle = \sqrt{6}\ell_0$. Under these assumptions, we have [38]

$$b(Q) = \frac{Q^2 \ell_0^2}{1 + Q^2 \ell_0^2}. \quad (15)$$

Note that for $Q\ell_0 \rightarrow 0$, $b(Q) \rightarrow Q^2 \ell_0^2$. In that limit, $S_{self}^{jump,SD}(Q,t)$ has a Gaussian form with an associated mean squared displacement that increases proportional to the time. Glass-forming systems exhibit stretched exponential forms for the self-correlation function [Eq. (1)]. An incoherent scattering function analogous to that for the simple jump diffusion [Eq. (13)] may be built by introducing the stretching in the time-dependent part:

$$S_{self}^{jump}(Q,t) = \exp\left[-b(Q)\left(\frac{t}{\tau_0'}\right)^\beta\right]. \quad (16)$$

In this way, in the limit $Q\ell_0 \rightarrow 0$ the Gaussian approximation is recuperated; but now a sublinearly increasing mean square displacement would be obtained for small- Q values, as observed from experiments and simulation. The resulting characteristic time is then given by

$$\tau_w = \tau_0' \left[1 + \frac{1}{Q^2 \ell_0^2}\right]^{1/\beta}, \quad (17)$$

which in the asymptotic low- Q limit is just $\tau_w \propto Q^{-2/\beta}$ [Eq. (3)]. This simple idea was, in fact, already worked out by us in the case of a sublinear diffusion in order to explain slight deviations previously found from Eq. (3) at high- Q values in PVME [11]. This model was also applied to previous PId3 results [30]. In that work, a value of $\ell_0 = 0.42 \text{ \AA}$ was found from a BS investigation of the α relaxation in PId3 at 270 K. Though the Q -range explored in that study was quite narrow ($Q \leq 1.9 \text{ \AA}^{-1}$), our results, obtained in a much wider Q range, can perfectly be described by such a model with the same value of ℓ_0 . This is shown in Fig. 8(b), where the dashed-dotted line is a fit with Eq. (17) (exponentiated to β) and the value of ℓ_0 fixed to 0.42 \AA . At the reference temperature of 300 K, for the only adjustable parameter the result $\tau_0'[ns] = 0.167^{1/\beta}$ is obtained. We can thus conclude that the experimental results on this polymer are compatible with a scenario of sublinear diffusion for the segmental relaxation with an underlying distribution of elemental jump lengths with a most probable value of $\ell_0 \approx 0.42 \text{ \AA}$. From Fig. 13, we further conclude that the jump distribution appears to be very little affected by temperature. All the curves corresponding to relaxation times simulated over a wide temperature range collapse onto a single master curve.

We can now ask whether this model also accounts for other observables accessed by the simulations, as α_2 . To obtain α_2 for this model, the total expression used for describing the self-correlation function has to be considered. It consists of the incoherent scattering function for jump anomalous diffusion [Eqs. (16) and (15)] affected by the pre-factor $A(Q)$ [Eq. (2)]:

$$S_{self}(Q,t) = \exp\left(-\frac{\langle u^2 \rangle}{3} Q^2\right) \exp\left[-\left(\frac{Q^2 \ell_0^2}{1 + Q^2 \ell_0^2}\right)\left(\frac{t}{\tau_0'}\right)^\beta\right]. \quad (18)$$

For small values of the variable $Q^2 \ell_0^2$, Eq. (18) can be approximated as

$$S_{self}(Q,t) = \exp\left[-\frac{\langle u^2 \rangle}{3} Q^2 - Q^2 \ell_0^2 \left(\frac{t}{\tau_0'}\right)^\beta\right] \times (1 - Q^2 \ell_0^2 + \dots). \quad (19)$$

Comparing this with the general expression for the expansion of $S_{self}(Q,t)$ in Q (see, e.g., Ref. [39])

$$S_{self}(Q,t) = \exp\left[-\frac{\langle r^2(t) \rangle}{6} Q^2 + \frac{\alpha_2(t) \langle r^2(t) \rangle^2}{72} Q^4 + \dots\right], \quad (20)$$

the following results are obtained for $\langle r^2(t) \rangle$ and $\alpha_2(t)$:

$$\langle r^2(t) \rangle = 2\langle u^2 \rangle + 6\ell_0^2 \left(\frac{t}{\tau_0'}\right)^\beta, \quad (21)$$

$$\alpha_2(t) = \frac{72\ell_0^4 \left(\frac{t}{\tau_0'}\right)^\beta}{\left[2\langle u^2 \rangle + 6\ell_0^2 \left(\frac{t}{\tau_0'}\right)^\beta\right]^2}. \quad (22)$$

In order to compare the results of Eqs.(21) and (22) with those of the simulations, the values of the different parameters involved have to be known for 320 K, the equivalent temperature to the 363 K of the simulations [2]. From the results obtained by IN13 for $\langle u^2 \rangle$, a linear temperature dependence extrapolates to $\langle u^2 \rangle \approx 0.66 \text{ \AA}^2$ at 320 K. ℓ_0 is assumed to be temperature independent in a first approximation. With the shape parameter found in the simulations $\beta = 0.4$ and using the appropriate a_T value ($a_{320 \text{ K}} = 0.42$), $\tau_0' = 1.3 \text{ ps}$ is obtained. The so calculated values for $\langle r^2(t) \rangle$ and $\alpha_2(t)$ are plotted in Fig. 14 as lines. As may be appreciated, a semiquantitative agreement is found between the values obtained from the model of anomalous diffusion with a distribution of jump lengths and those resulting from the simulations. Naturally, the comparison applies only to time scales

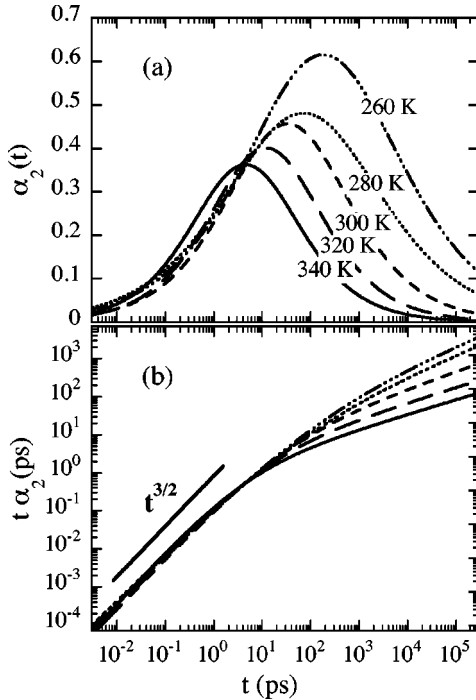


FIG. 15. Time evolution of the non-Gaussian parameter α_2 as predicted by the anomalous jump diffusion model with the parameters obtained from the quasielastic neutron scattering results on polyisoprene for the temperatures indicated. Figure (b) shows the data in (a) multiplied by the time.

longer than the characteristic for the fast dynamics, since the fast process has been simply parameterized by the LMF [Eq. (2)], i.e., through the effective contribution to the displacement characterized by $\langle u^2 \rangle$. In the range of applicability ($t \gtrsim 1$ ps) the shape and the position of the peak of $\alpha_2(t)$ are quite similar for both sets of data.

With this result at hand, we now exploit the model further in order to see whether it is able to reproduce the main features on $\alpha_2(t)$ that are reported in the literature from simulations of glass-forming systems, in general. Figure 15 shows the T dependence of $\alpha_2(t)$ calculated taking into account the values experimentally determined for PI for the different parameters involved in the model. At a first sight, it becomes evident the qualitative similarity shown by the so calculated non-Gaussian parameter with the data usually reported in the literature (see, e.g., Refs. [34,40–44]). Moreover, we can check whether this model also accounts for other seemingly universal features of α_2 : (i) In the asymptotic short time limit, $t\alpha_2(t) \propto t^{3/2}$, as pointed out by Caprion *et al.* [42]; (ii) the time t^* where the maximum of α_2 occurs shifts with τ_w ; (iii) the magnitude of α_2 increases with decreasing temperature.

(i) First of all, Fig. 15(b) explores the prediction of Caprion *et al.* [42]: the collapse of $t\alpha_2(t)$ in the short time regime to a universal function proportional to $t^{3/2}$. As can be seen in this figure, such behavior is very fairly reproduced by the simple anomalous jump diffusion model with the parameter values obtained for PI. This is not surprising since Eq. (22) delivers a t^β dependence for the short time asymptotic limit of $\alpha_2(t)$. As the β values obtained for our sample are

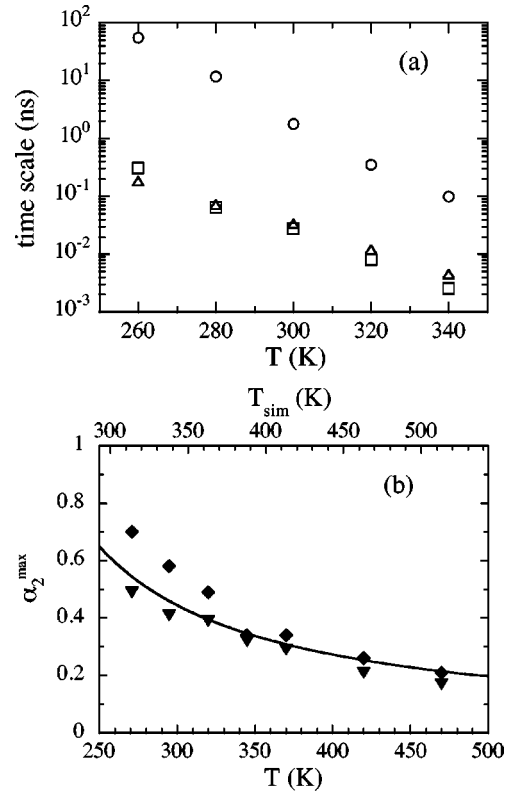


FIG. 16. Temperature dependence of (a) t^* (Δ), τ'_0 (\square), and $\tau'_w(Q=0.9 \text{ \AA}^{-1})$ (\circ) from the experiments and (b) the maximum value of α_2 , $\alpha_2^{\max} = \alpha_2(t^*)$, as obtained from the anomalous diffusion jump model with the experimental parameters determined for polyisoprene (solid line) and from the simulations for the main chain protons (diamonds) and for the main chain carbons (triangles). The temperature scale for the model data has been shifted 43 K to match that of the simulations.

close to 0.5—and usually so they are for polymers, in general—it is evident that this simple model accounts for such a feature. This means, while the stretching parameter takes values close to 0.5, the model here proposed reproduces the asymptotic limit reported in Ref. [42]. In that work, we note that for the selenium data shown the value of the β parameter was $\beta=0.53$ [45], and thus the anomalous jump diffusion model would also perfectly give account for the behavior found. In the case of the other system investigated in that work—a binary Lennard-Jones liquid—the slope of the curve $t\alpha_2(t)$ decreases asymptotically in a steeper way than $t^{3/2}$; no information on the value of the β parameter is given for this kind of system.

(ii) From Eq. (22) it is straightforward to calculate t^* as the time, where $\alpha_2(t)$ exhibits its maximum. We arrive at $t^* = \tau'_0 (\langle u^2 \rangle / 3\ell_0^2)^{1/\beta}$. Given the weak temperature dependencies of $\langle u^2 \rangle$ and β , to a good approximation the temperature dependence of t^* follows that of τ'_0 . Using the experimental parameters, Fig. 16(a) displays t^* and τ'_0 as a function of temperature. Both times are basically identical— t^* agrees nearly quantitatively with the jump time τ'_0 —a very plausible result. Moreover, Fig. 16(a) also shows that the temperature dependence of $t^*(T)$ is approximately the same as

that of $\tau_w(T)$. This is naturally understood because, according to Eq. (17), the temperature dependence of τ_w and τ_0' are the same apart from the slight changes of β with temperature.

(iii) Inserting t^* into Eq. (22), $\alpha_2^{max} = \alpha_2(t^*) = 3\ell_0^2/2\langle u^2 \rangle$ is obtained. With ℓ_0 approximately constant and $\langle u^2 \rangle$ decreasing linearly with T , α_2^{max} increases significantly with decreasing temperature. The values of α_2^{max} calculated by using the experimentally determined values for the parameters involved in the model are shown in Fig. 16(b) in comparison with the MD-simulation results at different temperatures. The temperature scale has been shifted in order to compatibilize neutron scattering and MD-simulation results. We note that the agreement between the model predictions and the simulations is good for the results on both the main chain protons and main chain carbons.

We can thus conclude that the main “universal” features reported in the literature for $\alpha_2(t)$ are well reproduced by a simple anomalous jump diffusion model with a distribution of jump lengths.

Now we can discuss the implications of the anomalous jump diffusion concerning the so-called heterogeneity of the α relaxation. First of all, we can say that the above mentioned model, in fact, involves a heterogeneous picture for the self-atomic motions in the α -relaxation regime which manifests at short length scales. There, each atom can jump over different distances at each moment; therefore, at large Q , where the neutron wave packet interacts only along a single step of the diffusion process, the system looks heterogeneouslike and non-Gaussianity is evident. However, for small Q , the contributions to $S_{self}(Q, t)$ originate from a large space volume of size $\sim 1/Q$; the scattering process observes the motion over long paths, i.e., over many diffusive elemental steps. Then, the result does not depend on the nature of the single step: at large scales the sublinear regime is reached and the system becomes Gaussian. This may be quantified furthermore in taking t^* , the time where $\alpha_2(t)$ displays its maximum, as a measure of the “lifetime” of the heterogeneous behavior. From the simulation results at 363 K (corresponding to experimental results at about 320 K), we can see that $\tau_w \sim t^*$ only for Q values of the order of 3 \AA^{-1} . At Q values of the order of 0.8 \AA^{-1} , $\tau_w \sim 25t^*$.

We note that in the jump diffusion scenario the origin of the stretching of the α relaxation is not addressed, since the sublinear diffusion is just assumed for reproducing the experimental findings. However, from the experimental simultaneous observation of sublinear diffusion and Gaussian behavior at $Q \leq Q_{max}$, a conclusion can be drawn: the stretching of the α process cannot be a consequence of a simple distribution of single exponentials. This was already demonstrated in Ref. [5]. Thus, the existence of a distribution of jump lengths may explain the deviations from Gaussian behavior at $Q \geq Q_{max}$ but is, in principle, decoupled from the origin of the stretching of the α relaxation. Furthermore, the semiquantitative agreement between the results obtained for α_2 from the simulations and the jump anomalous diffusion model suggests that the origin of the α_2 peak found in simulations of glass-forming systems (see, e.g., Refs. [34,40–44])

and which is usually attributed to the heterogeneity of the α process, might be simply due to a jump length distribution.

Finally, we would like to remark that the scenario of anomalous jump diffusion is, in principle, compatible with the MCT. The jumps leading to the sublinear diffusion would correspond to the dynamics allowing the decaging mechanism. In the framework of the MCT, a first estimation of the so-called mean characteristic localization length r_{sc} was done starting from the simulations at 363 K [2]. This was obtained from the value of the mean squared displacement at t^* , $\langle r^2(t^*) \rangle$ and assuming that $\langle r^2(t^*) \rangle \approx 6 r_{sc}^2$. This gives $r_{sc} \approx 0.45 \text{ \AA}$. It is worth remarking that the value found for $\ell_0 \approx 0.42 \text{ \AA}$ is in the range of that estimated for r_{sc} . This finding would suggest to identify the most probable jump distance ℓ_0 with the mean characteristic localization length. On the other hand, the value of the total mean squared displacement $\langle u^2 \rangle$ measured at IN13 also comprises the fast H librations and vibrations that are not part of the caging process. The $\langle u^2 \rangle$ associated with the fast dynamics (caging) could be significantly smaller (see, e.g., Fig. 15 of Ref. [15]). In any case, the most important criterion for jump diffusion, the separation of time scales (picosecond vs nanosecond), is well fulfilled.

VI. CONCLUSIONS

In combining the spin echo spectrometers IN11C and the Jülich NSE with the thermal backscattering instrument IN13 on a main chain protonated polyisoprene sample, we have performed a careful investigation on the Q dependence of the scattering function in the α -relaxation regime. At 300 K, we have been able to characterize the dynamics in the Q range $0.34 \leq Q \leq 4.7 \text{ \AA}^{-1}$. Combining the results from different temperatures, the Q range has been extended towards lower values as low as 0.1 \AA^{-1} . The experimental effort clearly established the crossover from Gaussian to non-Gaussian behavior of the α -relaxation scattering function. This crossover takes place at around $Q = 1.3 \text{ \AA}^{-1}$, close to the first maximum of the static structure factor. The results corroborate findings of earlier MD simulations performed on PI by some of us [2]. From the combination of the MD simulations and the experiment, a simple picture of the diffusion process underlying the α -relaxation evolved.

(i) At low Q corresponding to larger distances, we deal with a homogeneous sublinear diffusion process. This result is by now supported by a number of detailed investigations into the relationship between the shape of the relaxation function and the Q dispersion of the characteristic relaxation times.

(ii) At higher Q the relationship between shape and dispersion relation demanded by Gaussianity breaks down and a weaker dispersion is found.

(iii) The changing Q dispersion may be explained in terms of a sublinear jump diffusion model featuring a distribution of jump lengths. The distribution, thereby, seems to vary very little with temperature. From this model a non-Gaussianity parameter $\alpha_2(t)$ may be calculated which agrees very well with simulation.

(iv) This good agreement suggests that, at least to a reasonable approximation, the apparent non-Gaussianity observed for the α process at short enough times is indeed a result of a diffusion process with a distribution of finite jump lengths.

(v) The predicted non-Gaussian parameter from the jump diffusion model is able to reproduce the main conjectures that are reported in the literature from the simulations of glass forming systems, in general. These are the following.

(a) The time t^* where the maximum of α_2 occurs approximately shifts with τ_w .

(b) The magnitude of α_2 increases with decreasing T .

(c) In the asymptotic short time regime $t\alpha_2(t) \approx t^{3/2}$.

(vi) Seemingly the jump diffusion model captures the universal properties shown by so different glass formers as

ortho-terphenyl, water, polymers, selenium, and Lennard-Jones liquids.

ACKNOWLEDGMENTS

We thank Dr. L. Willner for the sample synthesis and Dr. M. Bee for experimental support at IN13. A.A., J.C., and F.A. acknowledge support from the following Project Nos.: DGICYT, PB97-0638; GV, EX 1998-23; UPV/EHU, 206.215-G20/98; 9/UPV 00206.215-13568/2001. Support from “Donostia International Physics Center” is also acknowledged by A.A., J.C., F.A., and D.R. The experiments at FZ Jülich were supported by the European Commission under the “Access to Research Infrastructures Action of the Human Potential Program: Contract No. HPRI-2001-0268.”

-
- [1] S.W. Lovesey, *Theory of Neutron Scattering from Condensed Matter* (Clarendon Press, Oxford, 1984).
- [2] J. Colmenero, F. Alvarez, and A. Arbe, Phys. Rev. E **65**, 041804 (2002).
- [3] J. Colmenero, A. Alegría, A. Arbe, and B. Frick, Phys. Rev. Lett. **69**, 478 (1992).
- [4] J. Colmenero, A. Arbe, A. Alegría, and K.L. Ngai, J. Non-Cryst. Solids **172-174**, 229 (1994).
- [5] A. Arbe, J. Colmenero, M. Monkenbusch, and D. Richter, Phys. Rev. Lett. **81**, 590 (1998).
- [6] O. Ahumada, D.N. Theodorou, A. Triolo, V. Arrighi, C. Karatasos, and J.P. Ryckaert, *Macromolecules* **35**, 7110 (2002).
- [7] W. Götze and L. Sjögren, Rep. Prog. Phys. **55**, 241 (1992).
- [8] M. Fuchs, J. Non-Cryst. Solids **172-174**, 241 (1994).
- [9] M. Fuchs, W. Götze, and M.R. Mayr, Phys. Rev. E **58**, 3384 (1998).
- [10] H. Sillescu, J. Non-Cryst. Solids **243**, 81 (1999).
- [11] J. Colmenero, A. Arbe, A. Alegría, M. Monkenbusch, and D. Richter, J. Phys.: Condens. Matter **11**, A363 (1999).
- [12] B. Farago, A. Arbe, J. Colmenero, R. Faust, U. Buchenau, and D. Richter, Phys. Rev. E **65**, 051803 (2002).
- [13] A. Arbe, J. Colmenero, F. Alvarez, M. Monkenbusch, D. Richter, B. Farago, and B. Frick, Phys. Rev. Lett. **89**, 245701 (2002).
- [14] B. Frick, D. Richter, and C. Ritter, Europhys. Lett. **9**, 557 (1989).
- [15] D. Richter, A. Arbe, J. Colmenero, M. Monkenbusch, B. Farago, and R. Faust, *Macromolecules* **31**, 1133 (1998).
- [16] U. Buchenau, M. Monkenbusch, M. Stamm, C. F. Majkrzak, and N. Nücker, in *Polymer Motion in Dense Systems*, edited by D. Richter and T. Springer, Springer Proceedings in Physics, Vol. 29 (Springer, Berlin, 1988).
- [17] B. Frick, D. Richter, R. Zorn, and L.J. Fetters, J. Non-Cryst. Solids **172-174**, 272 (1994).
- [18] R. Zorn, D. Richter, B. Farago, B. Frick, F. Kremer, U. Kirst, and L.J. Fetters, *Physica B* **180&181**, 534 (1992).
- [19] F. Alvarez, J. Colmenero, R. Zorn, L. Willner, and D. Richter, *Macromolecules* **36**, 238 (2003).
- [20] F. Alvarez, A. Arbe, and J. Colmenero, Chem. Phys. **261**, 47 (2000).
- [21] R. Zorn, B. Frick, and L.J. Fetters, J. Chem. Phys. **116**, 845 (2002).
- [22] G. L. Squires, *Introduction to the Theory of Thermal Neutron Scattering* (Dover, New York, 1996).
- [23] T. Springer, in *Quasielastic Neutron Scattering for the Investigation of Diffusive Motions in Solids and Liquids*, Springer Tracts in Modern Physics, Vol. 64 (Springer-Verlag, Berlin, 1972).
- [24] A. Rahman, K.S. Singwi, and A. Sjölander, Phys. Rev. **126**, 986 (1962).
- [25] V.F. Sears, *Neutron News* **3**, 26 (1992).
- [26] F. Alvarez, A. Arbe, J. Colmenero, R. Zorn, and D. Richter, J. Comput. Mater. Sci. **25**, 596 (2002).
- [27] F. Mezei, in *Neutron Spin Echo*, Lecture Notes in Physics, Vol. 28 (Springer-Verlag, Heidelberg, 1980).
- [28] R. Zorn, A. Arbe, J. Colmenero, B. Frick, D. Richter, and U. Buchenau, Phys. Rev. E **52**, 781 (1995).
- [29] W. Götze, in *Liquids, Freezing and Glass Transition*, edited by J.P. Hansen, D. Levesque, and J. Zinn-Justin (North-Holland, Amsterdam, 1991), p. 287.
- [30] A. Arbe, A. Alegría, J. Colmenero, S. Hoffmann, L. Willner, and D. Richter, *Macromolecules* **32**, 7572 (1999).
- [31] J. Colmenero, A. Arbe, and A. Alegría, J. Non-Cryst. Solids **172-174**, 126 (1994).
- [32] S. Hoffmann, L. Willner, D. Richter, A. Arbe, J. Colmenero, and B. Farago, Phys. Rev. Lett. **85**, 772 (2000).
- [33] S. Hoffmann, Ph.D. thesis, Westfälischen Wilhelms Universität Münster, 2000.
- [34] S. Mossa, R.D. Leonardo, G. Ruocco, and M. Sampoli, Phys. Rev. E **62**, 612 (2000).
- [35] H. Sun, J. Phys. Chem. B **102**, 7338 (1998).
- [36] G.D. Smith, W. Paul, M. Monkenbusch, L. Willner, D. Richter, X.H. Qiu, and M.D. Ediger, *Macromolecules* **32**, 8857 (1999).
- [37] K.S. Singwi and A. Sjölander, Phys. Rev. **119**, 863 (1960).
- [38] *An Introduction to the Liquid State*, edited by P.A. Egelstaff (Oxford University Press, New York, 1992).
- [39] R. Zorn, Phys. Rev. B **55**, 6249 (1997).
- [40] W. Kob and H.C. Andersen, Phys. Rev. E **51**, 4626 (1995).
- [41] W. Kob, C. Donati, S.J. Plimpton, P.H. Poole, and S.C. Glotzer, Phys. Rev. Lett. **79**, 2827 (1997).

- [42] D. Caprion, J. Matsui, and H.R. Schober, Phys. Rev. Lett. **85**, 4293 (2000).
- [43] M.M. Hurley and P. Harrowell, J. Chem. Phys. **105**, 10 521 (1996).
- [44] S. Kämmerer, W. Kob, and R. Schilling, Phys. Rev. E **58**, 2131 (1998).
- [45] D. Caprion, J. Matsui, and H.R. Schober, Phys. Rev. B **62**, 3709 (2000).